

Probing Supergranular Flow in the Solar Interior

M. F. Woodard

*Colorado Research Associates Division,
NorthWest Research Associates, Inc.,
3380 Mitchell Lane, Boulder, CO 80301-5410
mfw@cora.nwra.com*

ABSTRACT

Helioseismic correlation data computed from *SOHO*/MDI high-resolution Doppler images were inverted for solar subsurface supergranular flow, using an improved forward model. The statistical error of the inversion is set by the stochastic nature of solar wave excitation which limits the detection of supergranular flow with these data to the first four or five megameters below the photosphere. The photospheric supergranulation pattern, averaged over the ≈ 34 -hour duration of the data set, is found to persist over the detectable depth range. Contrary to some recent findings, there is no indication of a flow reversal at a depth between five and six megameters. However, since the depth of the putative reversal is at the edge of the detectable range for these data, the discrepancy is probably not significant.

Subject headings: Sun: interior; Sun: mass flows; Sun: helioseismology

1. INTRODUCTION

Supergranulation is one of several cellular flow patterns which have either been observed or proposed to exist in the Sun. Discovered about fifty years ago (Hart 1954, 1956) in photospheric Doppler measurements, supergranular flow is a patchwork of roughly 30 Mm-scale cells with lifetimes of order one day (Leighton et al. 1962). Individual cells are regions of horizontal flow, with typical speeds away from cell centers of a few hundred meters per second. Neighboring cells are separated by narrow lanes of converging gas, which coincide with the magnetic network (Simon & Leighton 1964). The observed photospheric outflow pattern and the constraint of mass conservation suggest a simple picture of overturning cells with gas rising to the photosphere at their centers, streaming outward, sinking at the boundaries, then returning to the surface (e.g. Parker 1973, Fig. 3). Supergranular motion

contributes a broad but distinct peak centered near spherical harmonic degree $\ell = 120$ in the wave number spectrum of photospheric convection (Hathaway et al. 2000, and references therein). Unlike the much smaller-scale and shorter-lived granulation pattern, which is known to play an important role in transporting the Sun’s luminosity to the photosphere, the role of supergranulation in transporting heat is not understood.

The existence of a supergranular scale of motion seems to have been unanticipated by theory and subsequent observations have provided additional surprises. For instance, it has been known for some time that the rotation rate of the supergranulation pattern exceeds that of the gas (Duvall 1980; Snodgrass & Ulrich 1990; Beck & Schou 2000) by a few percent. More recently, Gizon et al. (2003a,b) and Schou (2003) examined the horizontal wave vector-frequency spectrum of the observed supergranular velocity field and found it to be highly anisotropic. Interpreting the spectrum in terms of waves, they found more power near the solar equator in traveling-wave components moving with the solar rotation than against it. The observed power anisotropy accounts for the phenomenon of superrotation, though the nature of the waves and the underlying cause of the anisotropy have yet to be addressed. As an alternative explanation, Rast et al. (2004) and Lisle et al. (2004) proposed that the highly anisotropic supergranulation spectrum consists of supergranular and mesogranular ‘non-wave’ components, with different pattern velocities and influenced by a superrotating giant-cell pattern (Miesch et al. 2000).

A number of ideas have been put forward to account for the existence of a preferred, ~ 30 -Mm scale of convection. The idea that supergranular motions are driven in the He II ionization zone at ~ 20 -Mm depth was suggested not long after their discovery (Simon & Leighton 1964) and dominated the thinking for a long time. Early theoretical analyses suggested that the horizontal and vertical dimensions of the cells should be similar (Simon & Weiss 1968; Vickers 1971; Parker 1973), providing an obvious link between the depth of the He II layer and the horizontal dimension of the cells. A more recent line of thinking is that supergranular motions are organized close to the photosphere. In the Rast (2003) model, for example, mutually advecting granular downflow plumes produce a cellular pattern with a preferred scale. Crouch et al. (2006) have shown how a preferred horizontal scale can emerge in a model of colliding, aggregating photospheric magnetic elements, though a mechanism for producing a flow has not been identified. Realistic numerical simulations of near-surface convection are beginning to model supergranular-scale flow (Benson et al. 2005; Stein et al. 2006). The latest simulations reproduce the main trends in the observed wave number spectrum of surface convection reasonably well (Georgobiani et al. 2007). However, further comparison of simulation output and velocity observations is necessary to establish whether power spectra of simulated flows contain the detailed signatures, e.g., the broad peak of power observed at $\ell \approx 120$, of supergranulation.

Local helioseismic techniques, which exploit solar p - and f -mode oscillations, are beginning to reveal the vertical structure of supergranular flow. The first helioseismic measurements of supergranulation, based on the time-distance approach, suggested a pattern depth of two to three Mm (Kosovichev & Duvall 1997). Subsequent analyses (Duvall 1998; Zhao & Kosovichev 2003) yielded pattern depths between 8 and 15 Mm, based on the correlation between the inferred flow velocity near the photosphere and at depth. A noteworthy feature of these analyses is a reversal of the sign of the correlation coefficient between the flow at depth and the surface flow, which occurs at a depth of five to six Mm. The reversal has been taken as an indication of a return flow, consistent with the simple picture of overturning cells mentioned above. Braun & Lindsey (2003); Braun et al. (2004), using methods of helioseismic holography, also found an apparent counter flow, at a subphotospheric depth greater than about ten Mm. However, they attribute their deep flow signature to a leakage effect from the surface. They believe their results are consistent with a relatively shallow flow.

A newer approach to local helioseismic analysis directly exploits the correlation between distinct horizontal wave vector and frequency components of the observable wave field caused by flows and other space- and time-varying structure. Woodard (2002) performed an inversion for supergranular flow using correlation data computed from *SOHO*/MDI Doppler image sequences (Scherrer et al. 1995). The analysis, which served mainly to illustrate the method, used high-degree f -mode data. As these modes probe only a few Mm beneath the photosphere, no attempt was made to characterize the depth dependence of the flow and the analysis furthermore looked only at the steady component of the flow.

The analysis of supergranular flow described in this paper generalizes the Woodard (2002) analysis to describe both depth- and time-dependent flow. Increased depth coverage is made possible through the use of both p -mode data and more extensive f -mode data. Section 2 describes the Subtractive Optimally Localized Averages (SOLA) inversion algorithm used to map supergranular-scale flow. The analysis of a datacube of MDI helioseismic Doppler images, aimed at characterizing the depth dependence of the flow, is described in Section 3. The final section discusses directions for future research.

2. SOLA/MCD Inversions for the Horizontal Flow Divergence

Knowing how observational data depend on the state of the solar interior, i.e., having a *forward model*, is crucial to the rigorous analysis of correlation data. The Woodard (2002) analysis employed a forward model for a depth- and time-independent supergranular flow and did not treat error. The model was based on a picture of stochastically-excited waves

interacting with weak flows superimposed on a realistic static plane-parallel solar background model. Forward models have subsequently been developed to deal with flows having both depth and (slow) time dependence. As in the Woodard (2002) treatment, the expected dependence of helioseismic data is computed to linear order in the flow velocity (Woodard 2006; Gizon & Birch 2005). Linear dependence is expressed via a sensitivity kernel. The neglect of nonlinear terms in forward model calculations entails the Born approximation, the accuracy of which has been estimated to be roughly 10 % for supergranular flows (Birch & Felder 2004). Recent forward modeling (Gizon & Birch 2004) also quantifies the noise of helioseismic measurements, in terms of a data covariance matrix. The present inversion uses the Woodard (2006) forward model, as summarized in the Appendices, to compute the sensitivity of correlation data to subsurface flow and the Gizon & Birch (2004) model to compute data covariances.

The validity of the linearized forward model means that well-known linear inverse methods used in helioseismology can be applied to correlation data as well as to more traditional data types. Woodard (2002) used a simple linear least-squares fitting algorithm to infer the subsurface flow velocity. This section describes an SOLA method (Pijpers & Thompson 1992, 1994) for estimating the depth and time dependence of supergranular flow. The SOLA method used here takes correlation data in a compressed form and yields an estimate of the divergence, $D = \partial_x u_x + \partial_y u_y$, of the horizontal component of the flow velocity field, \mathbf{u} .

The treatment of small perturbations about a static and plane-parallel background model is simplified by working in the Fourier domain. Raw Fourier-domain correlation data are simple products of the horizontal-wave-vector \mathbf{k} and temporal-frequency ω components, $\varphi_{\mathbf{k}\omega}$, of the observed photospheric Doppler signal. The sensitivity of these data to poloidal flow, parameterized according to equation (A1), is given by equation (A4). The inversion described below uses correlation data in the compressed form $\beta_{m\mathbf{q}\sigma}$ defined by equation (A8), where the indices \mathbf{q} and σ denote horizontal wave vector and frequency and m is the index of the vertical function $\gamma_m(z)$ in equation (A1). The sensitivity of the compressed data to poloidal flow is given by either of equations (A9) and (A10). The latter equation shows the expected value of $\beta_{m\mathbf{q}\sigma}$ to be a weighted integral over z of the Fourier component $D_{\mathbf{q}\sigma}(z)$ of the horizontal flow divergence D at height z . This form for the sensitivity kernel allows the z dependence of $D_{\mathbf{q}\sigma}(z)$ to be obtained by Multi-Channel Deconvolution (MCD, Jacobsen et al. 1999) using $\beta_{m\mathbf{q}\sigma}$ as input data.

In the MCD approach taken here, $D(z) \equiv D_{\mathbf{q}\sigma}(z)$ at height z is estimated from a linear combination

$$\tilde{D}(z) = \sum_{m=0}^M w_m^*(z) \beta_m \quad (1)$$

of the compressed data, $\beta_m \equiv \beta_{m\mathbf{q}\sigma}$, with weights w_m chosen to optimize the trade off between depth resolution and estimation noise. Note that for a given \mathbf{q} and σ there is one β_m for each of the $M + 1 = 9$ vertical components, γ_m , of the flow field. As the remainder of this section discusses the inversion for a single Fourier component of D , the subscripts \mathbf{q} and σ can be dropped. To compute the depth resolution of a flow estimate $\tilde{D}(z)$, at a particular depth, one needs to know how sensitive the estimate is to the actual flow $D(z')$ at all depths. Depth sensitivity is expressed by

$$E[\tilde{D}(z)] = \int R(z, z') D(z') dz', \quad (2)$$

where ‘ E ’ denotes statistical expectation. By equations (A10) and (1), the *averaging* kernel has the form

$$R(z, z') = \sum_{m=0}^M w_m^*(z) r_m(z'), \quad (3)$$

where $r_m(z) \equiv r_{m\mathbf{q}\sigma}(z)$ is the data sensitivity function. (In this paper, the limits on integrations over the vertical coordinate are always z_{\min}, z_{\max} , which define the vertical boundaries of the wave propagation domain, as described in §A.)

Optimally-localized averages are designed to provide a balanced mix of resolution and signal-to-noise. In the SOLA approach, depth resolution at sampling depth $|z|$, is gauged by the agreement between the $\tilde{D}(z)$ -dependent averaging kernel, $R(z, z')$, and a prescribed, target kernel $R_{\text{targ}}(z, z')$, the latter a strongly-peaked function of z' near z . For this work, the measure of mismatch between averaging and target kernels is

$$\mathcal{F}(\tilde{D}(z)) = \int |R_{\text{targ}}(z, z') - R(z, z')|^2 dz', \quad (4)$$

with the $\tilde{D}(z)$ ($w_m(z)$) dependence of $R(z, z')$ given by equation (3). Using the noise model outlined in §B as the basis for evaluating statistical uncertainty, a convenient measure of the noise in $\tilde{D}(z)$ is

$$\mathcal{G}(\tilde{D}(z)) = \text{Cov}[\tilde{D}(z), \tilde{D}(z)] = \sum_{m, m'=0}^M w_m^*(z) \alpha_{mm'} w_{m'}(z), \quad (5)$$

which follows from equations (B4) and (1), where the $\alpha_{mm'} \equiv \alpha_{m\mathbf{q}\sigma, m'\mathbf{q}\sigma}$ are elements of the curvature matrix, introduced through equation (A9). The balance between resolution and signal-to-noise at a particular z is achieved by choosing $\tilde{D}(z)$ (effected by choosing the parameters $w_m(z)$) to minimize $\mathcal{F} + \lambda \mathcal{G}$, where λ is a positive trade-off parameter. The $w_m(z)$ which minimize this function are obtained by solving the system

$$\sum_{m'=0}^M \left[\int r_m(z') r_{m'}^*(z') dz' + \lambda \alpha_{mm'} \right] w_{m'}(z) = \int R_{\text{targ}}(z, z') r_m(z') dz' \quad (6)$$

of linear equations, for $m = 0, M$, with $r_m(z)$ given by equation (A10).

3. Analysis and Results

An SOLA/MCD inversion for the horizontal divergence of supergranular-scale flow, as outlined in §2, was performed using helioseismic correlations derived from an ≈ 34 -hr sequence of *SOHO*/MDI high-resolution Doppler images obtained on 1999 May 31 – June 1. This data cube was also used in the Woodard (2002) supergranular flow inversion and covers an approximately 210×210 Mm² corotating patch of the photosphere near disk center. The signal, $\varphi_{\mathbf{k}\omega}$, used to construct correlation data was taken from trumpet-shaped regions of $\mathbf{k}\omega$ space centered on ridges of oscillatory power of different radial order. The selected region for a particular order n is defined to be all \mathbf{k} and ω such that ω is close to (i.e. within the full width $\gamma_{n\mathbf{k}}$ of) the mode frequency $\omega_{n\mathbf{k}}$. For a given order, the \mathbf{k} vectors are restricted to values for which the oscillation mode of order n and wave vector \mathbf{k} is resolved in the spectrum, as required by the assumptions of the sensitivity calculation (see §A). The selected regions of $k = |\mathbf{k}|$ and ω are shown in Figure 1.

The target kernels used to construct flow estimates were chosen to have the Gaussian form $R_{\text{targ}}(z, z') \propto \exp[-([z - z']/\Delta z)^2]$. For a given \mathbf{q} , σ , and z , sets of weights $w_m(z)$ were computed by solving equation (6) for a number of combinations of the trade-off parameter λ and target width Δz . The choice of λ and Δz for the inversion was made based on visual inspection of the resulting averaging kernels, $R(z, z')$, computed according to equation (3), to their target kernels and on the noise of the flow estimates, computed according to equation (5). With these choices, reasonably well-behaved averaging kernels can be constructed for sampling depths less than ten Mm. For a particular Δz , λ was chosen to minimize noise while maintaining faithfulness to the target kernel. Flow divergence estimates were obtained over the depth range zero to ten Mm, for \mathbf{q} of magnitude q in the angular degree range $qR_{\odot} \approx 50 - 155$ and for $\sigma = 0$ (i.e. for the steady component of the flow). Figure 2 depicts the averaging kernels used in the inversion for angular degree $qR_{\odot} \approx 60$ and $\sigma = 0$ (corresponding to a horizontal scale of approximately 70 Mm).

To explore the depth dependence of supergranular flow, I computed the cross power $Q(z, z')$ of the inferred flow divergence between different depths. $Q(z, z')$ is defined to be $\tilde{D}(\mathbf{x}, z, t)\tilde{D}(\mathbf{x}, z', t)$ averaged over the \mathbf{x}, t domain of the data cube, where $\tilde{D}(\mathbf{x}, z, t) = \sum_{\mathbf{q}\sigma} \tilde{D}_{\mathbf{q}\sigma}(z) \exp[i(\mathbf{q} \cdot \mathbf{x} - \sigma t)]$ is the inferred divergence field. Both solar flows and noise contribute to the observed cross power. Figure 3 shows the measured power, $Q(z, z)$, and its expected noise contribution, $\mathcal{G}(z)$, as functions of depth. Supergranular flow appears to dominate the observed power to a depth of four Mm. Below four Mm depth the supergranu-

lar contribution becomes somewhat uncertain, since it is not much larger than the estimated noise contribution. Below six Mm, the power is almost certainly noise dominated and the discrepancy between the measured power and expected noise power is most likely due to inadequacies of the noise model. As noted in §B, the noise model ignores both the limited sampling and the curvature of the photosphere. Hereafter, I consider only the first six Mm beneath the photosphere.

An improved estimate of supergranulation power was obtained by subtracting the theoretical noise power from the measured power and the resulting debiased power is shown in Figure 4. The estimated supergranulation power diminishes gradually with depth over the depth range shown. The debiased cross power $Q(0, z)$, also shown in Figure 4, is a measure of the correlation between the surface velocity field and the velocity field at depth. Note that the expected noise contribution to $Q(0, z)$ is negligible because the noise of the surface measurement is small. The z -dependence of the observed cross power is consistent with a flow pattern which is highly coherent over the depth range shown. Although there is no indication that the cross power changes sign between five and six Mm depth, the statistics of the measurement are probably not sufficient to rule out a reversal at these depths.

To examine vertical coherence more objectively, I computed the debiased expectations of $Q(z, z)$ and $Q(0, z)$ for hypothetical flows with divergence of the form $D_{\mathbf{q}\sigma}(z) \propto \exp[-(z/z_0)^2]$, for trial values of the penetration depth z_0 . The trial $D_{\mathbf{q}\sigma}(z)$ profiles, shown with the debiased $Q(z, z)$ and $Q(0, z)$ in Figure 5, were normalized to agree with the values at $z = 0$ obtained from the inversion. The curves which fit the observations best are for $z_0 \approx 6$ Mm, a value which is intermediate among the range of reported values, but not in agreement with any of them. Of course, the results presented in Figure 4 pertain to a specific set of (Gaussian profile) flow models which are used mainly for simplicity.

4. DISCUSSION AND OUTLOOK

The results of this analysis reinforce studies indicating that the photospheric supergranular flow pattern extends four or more megameters into the solar interior. The approximate agreement between theoretical noise power and measured power in the flow estimates at depths approaching ten Mm (Fig. 3) provides further confirmation that the noise of helioseismic measurements is set by the stochastic nature of wave excitation. Thus Figure 3 represents a significant challenge to detecting supergranular flow at depth, using a data cube with the dimensions of the cube used in the present analysis and with the mode set used in the analysis.

Analysis of large volumes of helioseismic data will substantially reduce the random error of the inversions, enabling us to measure convective power and cross power over a significantly greater range of depths than the zero to six Mm range obtainable with a single 34-hr data cube. To take full advantage of current and anticipated helioseismic data sets will require further improvements in the data sensitivity and noise model. For instance, the treatment of wave excitation and damping used for the current sensitivity calculations is somewhat simplistic and could be sharpened. Sources of systematic error include unmodeled features of the solar envelope, such as magnetic or sound-speed perturbations, and assumptions, such as the Born approximation, implicit in the sensitivity calculations. A potentially significant source of experimental error, which has yet to be addressed, is aliasing due to limited observational coverage of the solar disk. A proper treatment of aliasing will improve both the sensitivity calculations and the noise model, allowing us, for instance, to deal with oscillation modes which are spectrally unresolved.

Realistic simulations of supergranular convection (Benson et al. 2005; Stein et al. 2006) are also beginning to impact our understanding of subsurface supergranulation. In addition to the insights that they provide about the physics of convection, the simulations give us a way to test local helioseismic methods (e.g., Georgobiani et al. 2007). Inversions of simulated correlation data are expected to provide useful checks on the sensitivity and noise models.

I thank Yuhong Fan for participating in the forward-modeling calculations used for the inversion. I also acknowledge Aaron Birch and an anonymous referee for invaluable help with the manuscript. The Solar Oscillations Investigation-Michelson Doppler Imager experiment on *SOHO* is supported by NASA contract NAG5-3077 at Stanford University. *SOHO* is a project of international cooperation between ESA and NASA. This research was supported by the NSF under grant ATM 02-23127 and NASA under contract NNH06CD84C.

A. The Sensitivity Kernel for Correlation Data

For the sensitivity calculations, waves and flows are modeled in a propagation domain defined by $0 < x, y < L$, $z_{\min} < z < z_{\max}$, for an interval $0 < t < T$ of time, where $x, y, z = \mathbf{x}, z$ are Cartesian coordinates which track the local solar rotation such that z equals height above the $\tau_{5000} = 1$ level of the photosphere. The underlying structure of the background model is an adaptation of solar model S of Christensen-Dalsgaard et al. (1993). The upper boundary of the propagation domain is given by $z_{\max} = 0.479$ Mm and corresponds to the outermost grid point of the Christensen-Dalsgaard *et al.* model, while the lower boundary, given by $z_{\min} = -25$ Mm, was placed below the penetration depth of

waves considered in this analysis. Physical quantities which describe perturbations about the underlying model are represented by functions which obey periodic boundary conditions in the \mathbf{x}, t propagation domain. It is appropriate to work in Fourier space, using the convention $f(\mathbf{x}, t) = \sum_{\mathbf{k}\omega} f_{\mathbf{k}\omega} \exp[i(\mathbf{k} \cdot \mathbf{x} - \omega t)]$ for the discrete \mathbf{k} ($= k_x, k_y$), ω representation of physical functions. For instance, the Fourier components of the helioseismic Doppler signal will be denoted $\varphi_{\mathbf{k}\omega}$.

Woodard (2006) computed data sensitivity for poloidal and toroidal flows with vanishing mass flux divergence. In the present analysis the supergranulation pattern is modeled as a poloidal flow, even though some toroidal component has been observed (Gizon & Duvall 2003). Such a flow can be represented

$$\rho(z) \mathbf{u}_{\mathbf{q}\sigma}(z) = \sum_{m=0}^M a_{m\mathbf{q}\sigma} [\hat{\mathbf{z}}q^2 \gamma_m(z) + i\mathbf{q} \frac{d\gamma_m}{dz}], \quad (\text{A1})$$

where $\mathbf{u}_{\mathbf{q}\sigma}(z)$ is the $(\mathbf{k}, \omega) = (\mathbf{q}, \sigma)$ component of the flow velocity, \mathbf{u} , at height z above the photosphere, $\rho(z)$ is the mass density profile, $\gamma_m(z)$ are a set of vertical basis functions, and $a_{m\mathbf{q}\sigma}$ are arbitrary coefficients. For this work, the vertical functions are defined by $\rho^{-1} d\gamma_m/dz = t_m(z) = T_m(2[z - (z_{\min} + z_{\max})/2]/(z_{\min} - z_{\max}))$, where T_m are Chebyshev polynomials of the first kind, and by the condition $\gamma_m(z_{\max}) = 0$. The latter condition implies that the vertical mass flux vanishes at the top of the model domain. In the analysis described here, the expansion defined by equation (A1) was truncated at $M = 8$.

A quantity of physical interest is the divergence $D(\mathbf{x}, z, t) = \partial_x u_x + \partial_y u_y$ of the horizontal component of the flow velocity. A flow parameterized according to equation (A1) is completely determined by $D(\mathbf{x}, z, t)$, whose Fourier components are

$$D_{\mathbf{q}\sigma}(z) = i\mathbf{q} \cdot \mathbf{u}_{\mathbf{q}\sigma}(z) = -q^2 \sum_{m=0}^M a_{m\mathbf{q}\sigma} t_m(z). \quad (\text{A2})$$

This equation can be inverted to give

$$a_{m\mathbf{q}\sigma} = - \int U_m(z) D_{\mathbf{q}\sigma}(z) dz / q^2, \quad (\text{A3})$$

where $U_m(z)$ can be constructed from the $t_m(z)$ functions. In this paper, the z -integration interval is always $[z_{\min}, z_{\max}]$.

The direct-modeling inversion uses correlation data in the dimensionless form $\hat{\varphi}_{\mathbf{k}'\omega'} \hat{\varphi}_{\mathbf{k}\omega}^*$, with $\hat{\varphi}_{\mathbf{k}\omega} = \varphi_{\mathbf{k}\omega} / \sqrt{P_{\mathbf{k}\omega}}$, where $\varphi_{\mathbf{k}\omega}$ is the $\mathbf{k}\omega$ component of the Doppler signal and $P_{\mathbf{k}\omega} = E[|\varphi_{\mathbf{k}\omega}|^2]$ is the expected power spectrum (limit spectrum) of the signal. In this paper, $E[Q]$ denotes the statistical expectation of Q . The linear dependence of the expected value of the

correlation data on the flow parameters $a_{m\mathbf{q}\sigma}$ (the expansion coefficients of Eq. [A1]) can be written in the general form

$$E[\hat{\varphi}_{\mathbf{k}'\omega'} \hat{\varphi}_{\mathbf{k}\omega}^*] = \sum_{m=0}^M \mathcal{K}_{\mathbf{k}'\omega', \mathbf{k}\omega}^{(m)} a_{m(\mathbf{k}'-\mathbf{k})(\omega'-\omega)}, \quad (\text{A4})$$

with

$$\mathcal{K}_{\mathbf{k}'\omega', \mathbf{k}\omega}^{(m)} = \mathcal{X}_{\mathbf{k}'\omega', \mathbf{k}\omega}^{(m)} + \mathcal{X}_{\mathbf{k}\omega, \mathbf{k}'\omega'}^{(m)*}. \quad (\text{A5})$$

The sensitivity kernel for the present inversions was computed from the approximate expression (adapted from Woodard 2006, §4.2)

$$\mathcal{X}_{\mathbf{k}\omega, \mathbf{k}'\omega'}^{(m)} = - \sum_{n, n'=0}^4 \frac{w_{n\mathbf{k}\omega} R_{n\mathbf{k}\omega} S_{n\mathbf{k}\omega, n'\mathbf{k}'\omega'}^{(m)} P_{n'\mathbf{k}'\omega'}}{w_{n'\mathbf{k}'\omega'} \sqrt{P_{\mathbf{k}\omega} P_{\mathbf{k}'\omega'}}}. \quad (\text{A6})$$

The factor $P_{n\mathbf{k}\omega}$ in this expression is the contribution of oscillatory modes of radial order n and horizontal wave vector \mathbf{k} to the limit spectrum $P_{\mathbf{k}\omega}$. The factor $R_{n\mathbf{k}\omega} = 1/(\omega_{n\mathbf{k}}^2 - \omega^2 - i\omega\gamma_{n\mathbf{k}})$ characterizes the frequency-dependent response of a harmonically-driven, simple, damped oscillator of resonant frequency $\omega_{n\mathbf{k}}$ and damping rate $\gamma_{n\mathbf{k}}$ (the mode frequency and damping rate). The quantities $R_{n\mathbf{k}\omega}$, $P_{n\mathbf{k}\omega}$, and $P_{\mathbf{k}\omega} = \sum_n P_{n\mathbf{k}\omega}$ were computed from parameterized fits to oscillation power spectra. The factor $S_{n\mathbf{k}\omega, n'\mathbf{k}'\omega'}^{(m)}$, which quantifies the flow-dependent, dynamical coupling of the oscillation modes of orders n and n' and horizontal vectors \mathbf{k} and \mathbf{k}' , is a combination of integrals over depth involving oscillation eigenfunctions computed from the solar model. The quantity $w_{n\mathbf{k}\omega}$ equals $-i\omega O_{\mathbf{k}} V_{n\mathbf{k}}^{(o)}$, where $O_{\mathbf{k}}$ is the measured MDI optical transfer function described in Woodard (2006) and $V_{n\mathbf{k}}^{(o)}$ is the vertical component of the mode displacement eigenfunction at $z = 200$ km, the approximate height in the solar atmosphere where MDI observes oscillations.

A derivation and detailed discussion of the sensitivity kernel is given in Woodard (2006). To summarize, equation (A6) applies to non-magnetic regions of the Sun and was derived under the assumption that modes of different radial order are excited incoherently. Perturbations of the source and damping by supergranular flow (Jackiewicz et al. 2006) are not modeled. Furthermore, the sensitivity kernel is only appropriate for observations near the center of the solar disk, where the Doppler velocity is approximately equal to the vertical velocity of wave motion. Equation (A6) ignores leakage contributions, due to the limited field of view of the Doppler observations, to $E[\hat{\varphi}_{\mathbf{k}'\omega'} \hat{\varphi}_{\mathbf{k}\omega}^*]$. Spatial leakage correlation signatures have an approximate symmetry property which suppresses their effect on an inversion for flow. The spectral profiles of solar oscillations are effectively broadened by spatial leakage. Therefore, the form for the sensitivity kernel used in this work is of questionable validity for narrow, unresolved modes. Finally, since a plane-parallel model is used for the propagation medium, correlations due to the curvature of the real Sun have been ignored.

The data sensitivity can alternatively be written in the form

$$E[\hat{\varphi}_{(\mathbf{k}+\mathbf{q})(\omega+\sigma)} \hat{\varphi}_{\mathbf{k}\omega}^*] = \sum_{m=0}^M \mathcal{K}_{(\mathbf{k}+\mathbf{q})(\omega+\sigma),\mathbf{k}\omega}^{(m)} a_{m\mathbf{q}\sigma}, \quad (\text{A7})$$

displaying the decomposition of the kernel into a set of kernels, one for each $\mathbf{q}\sigma$ component of the flow. The decomposition permits a so-called Multi-Channel Deconvolution (MCD, Jacobsen et al. 1999), in which the flow parameters $a_{m\mathbf{q}\sigma}$ for different $\mathbf{q}\sigma$ are determined independently of one another from helioseismic data. Inversions based on equation (A7) can in principle be performed using ‘raw’ correlation data, $\hat{\varphi}_{(\mathbf{k}+\mathbf{q})(\omega+\sigma)} \hat{\varphi}_{\mathbf{k}\omega}^*$ directly. However, the present inversion uses only the combinations

$$\beta_{m\mathbf{q}\sigma} = \sum_{\mathbf{k}\omega} \mathcal{K}_{(\mathbf{k}+\mathbf{q})(\omega+\sigma),\mathbf{k}\omega}^{(m)*} \hat{\varphi}_{(\mathbf{k}+\mathbf{q})(\omega+\sigma)} \hat{\varphi}_{\mathbf{k}\omega}^* \quad (\text{A8})$$

of raw data. The motivation for working explicitly with $\beta_{m\mathbf{q}\sigma}$ comes from least-squares analysis, which requires only these combinations, equal to the components of the gradient of the χ^2 merit function minimized by the fit (Press et al. 1992, Ch. 15). The fact that least-squares analysis uses, in effect, a ‘compressed’ data set, suggests that most of the information about subsurface flow resides in $\beta_{m\mathbf{q}\sigma}$. Moreover, if the number of vertical basis functions γ_m is not terribly large (the present analysis uses $M + 1 = 9$ functions), then $\beta_{m\mathbf{q}\sigma}$ is a more compact and manageable data set to work with than the raw correlation data.

By equations (A7) and (A8), the sensitivity of the compressed data to the flow is given by

$$E[\beta_{m\mathbf{q}\sigma}] = \sum_{m'=0}^M \alpha_{m\mathbf{q}\sigma,m'\mathbf{q}\sigma} a_{m'\mathbf{q}\sigma}, \quad (\text{A9})$$

where $\alpha_{m\mathbf{q}\sigma,m'\mathbf{q}\sigma} = \sum_{\mathbf{k}\omega} \mathcal{K}_{(\mathbf{k}+\mathbf{q})(\omega+\sigma),\mathbf{k}\omega}^{(m)*} \mathcal{K}_{(\mathbf{k}+\mathbf{q})(\omega+\sigma),\mathbf{k}\omega}^{(m')}$ is the ‘curvature’ matrix of least-squares analysis. By equations (A3) and (A9), the sensitivity model for compressed data can also be expressed in terms of the horizontal flow divergence $D_{\mathbf{q}\sigma}(z)$:

$$E[\beta_{m\mathbf{q}\sigma}] = \int r_{m\mathbf{q}\sigma}(z) D_{\mathbf{q}\sigma}(z) dz, \quad (\text{A10})$$

where $r_{m\mathbf{q}\sigma}(z) \equiv -\sum_{m'=0}^M \alpha_{m\mathbf{q}\sigma,m'\mathbf{q}\sigma} U_{m'}(z)/q^2$.

B. The Noise Model

A quantitative model of random error plays a role both in defining the inversion procedure and in evaluating the uncertainty of the inferred flow. To estimate the noise of

helioseismic measurements, a number of investigators have treated the signal components $\varphi_{\mathbf{k}\omega}$ as independent complex Gaussian random variables (Gizon & Birch 2004, and references therein). The motivation for these statistics comes from the theory that solar oscillations are stochastically excited by small-scale subphotospheric turbulence. The Gizon and Birch noise model ignores the effect of the weak, flow-dependent correlations discussed in the previous section. In this analysis the effect of correlations introduced by the limited field of view of the observations and by the curvature of the solar surface will also be ignored.

Because the real-valued Doppler signal is subject to the constraint $\varphi_{-\mathbf{k},-\omega} = \varphi_{\mathbf{k}\omega}^*$, the assumption of independent variables can only hold for restricted sets of signal components. In this work, only positive-frequency components are considered. Even with this restriction, the correlation data are redundant because $\varphi_{\mathbf{k}'\omega'} \varphi_{\mathbf{k}\omega}^*$ and $\varphi_{\mathbf{k}\omega} \varphi_{\mathbf{k}'\omega'}^*$ are related by complex conjugation. Using the notation η_1, η_2, \dots to refer to a non-redundant set of dimensionless correlation data and following Appendix C of Gizon & Birch (2004), one obtains

$$\text{Cov}[\eta_i, \eta_j^*] = 0 \tag{B1}$$

and

$$\text{Cov}[\eta_i, \eta_j] = \delta_{ij}, \tag{B2}$$

where $\text{Cov}[a, b] \equiv E[ab^*] - E[a]E[b^*]$. These equations are equivalent to the statement that the covariance matrix of the real and imaginary parts of the correlation data is one-half the unit matrix. As a consequence of equations (A8), (B1), and (B2), the covariance matrix of the compressed data is given by

$$\text{Cov}[\beta_{m\mathbf{q}\sigma}, \beta_{m'\mathbf{q}'\sigma'}^*] = 0 \tag{B3}$$

and

$$\text{Cov}[\beta_{m\mathbf{q}\sigma}, \beta_{m'\mathbf{q}'\sigma'}] = \alpha_{m\mathbf{q}\sigma, m'\mathbf{q}'\sigma'}. \tag{B4}$$

REFERENCES

- Beck, J. G. & Schou, J. 2000, *Sol. Phys.*, 193, 333
- Benson, D., Stein, R., & Nordlund, A. 2005, AGU Spring Meeting Abstracts, C5
- Birch, A. C. & Felder, G. 2004, *ApJ*, 616, 1261
- Braun, D. C., Birch, A. C., & Lindsey, C. 2004, in *Proc. SOHO 14/GONG 2004 Workshop (ESA SP-559; Noordwijk: ESA)*, ed. D. Danesy, 337
- Braun, D. C. & Lindsey, C. 2003, in *Proc. SOHO 12/GONG 2002 (ESA SP-517; Noordwijk: ESA)*, ed. H. Sawaya-Lacoste, 15–22
- Christensen-Dalsgaard, J., Proffitt, C. R., & Thompson, M. J. 1993, *ApJ*, 403, L75
- Crouch, A. D., Charbonneau, P., & Thibault, K. 2006, in *AAS/Solar Physics Division Meeting*, 30.04
- Duvall, T. L., Jr. 1980, *Sol. Phys.*, 66, 213
- Duvall, T. L., Jr. 1998, in *Proc. SOHO 6/GONG 98 Workshop (ESA SP-418; Noordwijk: ESA)*, ed. S. Korzennik, 581
- Georgobiani, D., Zhao, J., Kosovichev, A. G., Benson, D., Stein, R. F., & Nordlund, Å. 2007, *ApJ*, 657, 1157
- Gizon, L. & Birch, A. C. 2004, *ApJ*, 614, 472
- . 2005, *Living Reviews in Solar Physics*, 2, 6
- Gizon, L. & Duvall, T. L., Jr. 2003, in *Proc. SOHO 12/GONG 2002 (ESA SP-517; Noordwijk: ESA)*, ed. H. Sawaya-Lacoste, 43
- Gizon, L., Duvall, T. L., Jr., & Schou, J. 2003a, *Nature*, 421, 43
- . 2003b, *Nature*, 421, 764
- Hart, A. B. 1954, *MNRAS*, 114, 17
- . 1956, *MNRAS*, 116, 38
- Hathaway, D. H., Beck, J. G., Bogart, R. S., Bachmann, K. T., Khatri, G., Petitto, J. M., Han, S., & Raymond, J. 2000, *Sol. Phys.*, 193, 299

- Jackiewicz, J., Gizon, L., & Birch, A. 2006, in Proc. SOHO 18/GONG 2006/HELAS I (ESA SP-624; Noordwijk: ESA), 52
- Jacobsen, B. H., Møller, I., Jensen, J. M., & Effersø, F. 1999, *Phys. and Chem. of the Earth*, 24, 215
- Kosovichev, A. G. & Duvall, T. L., Jr. 1997, in *ASSL Vol. 225: SCORE'96 : Solar Convection and Oscillations and their Relationship*, ed. F. P. Pijpers, J. Christensen-Dalsgaard, & C. S. Rosenthal, 241
- Leighton, R. B., Noyes, R. W., & Simon, G. W. 1962, *ApJ*, 135, 474
- Lisle, J. P., Rast, M. P., & Toomre, J. 2004, *ApJ*, 608, 1167
- Miesch, M. S., Elliott, J. R., Toomre, J., Clune, T. L., Glatzmaier, G. A., & Gilman, P. A. 2000, *ApJ*, 532, 593
- Parker, E. N. 1973, *ApJ*, 186, 643
- Pijpers, F. P. & Thompson, M. J. 1992, *A&A*, 262, L33
- . 1994, *A&A*, 281, 231
- Press, W. H., Teukolsky, S. A., Vetterling, W. T., & Flannery, B. P. 1992, *Numerical recipes in C. The art of scientific computing* (Cambridge: University Press, —c1992, 2nd ed.)
- Rast, M. P. 2003, *ApJ*, 597, 1200
- Rast, M. P., Lisle, J. P., & Toomre, J. 2004, *ApJ*, 608, 1156
- Scherrer, P. H., Bogart, R. S., Bush, R. I., Hoeksema, J. T., Kosovichev, A. G., Schou, J., Rosenberg, W., Springer, L., Tarbell, T. D., Title, A., Wolfson, C. J., Zayer, I., & MDI Engineering Team. 1995, *Sol. Phys.*, 162, 129
- Schou, J. 2003, *ApJ*, 596, L259
- Simon, G. W. & Leighton, R. B. 1964, *ApJ*, 140, 1120
- Simon, G. W. & Weiss, N. O. 1968, *Zeitschrift fur Astrophysik*, 69, 435
- Snodgrass, H. B. & Ulrich, R. K. 1990, *ApJ*, 351, 309
- Stein, R. F., Benson, D., Georgobiani, D., & Nordlund, Å. 2006, in Proc. SOHO 18/GONG 2006/HELAS I (ESA SP-624; Noordwijk: ESA), 79

Vickers, G. T. 1971, *ApJ*, 163, 363

Woodard, M. F. 2002, *ApJ*, 565, 634

—. 2006, *ApJ*, 649, 1140

Zhao, J. & Kosovichev, A. G. 2003, in *Proc. SOHO 12/GONG 2002* (ESA SP-517; Noordwijk: ESA), ed. H. Sawaya-Lacoste, 417

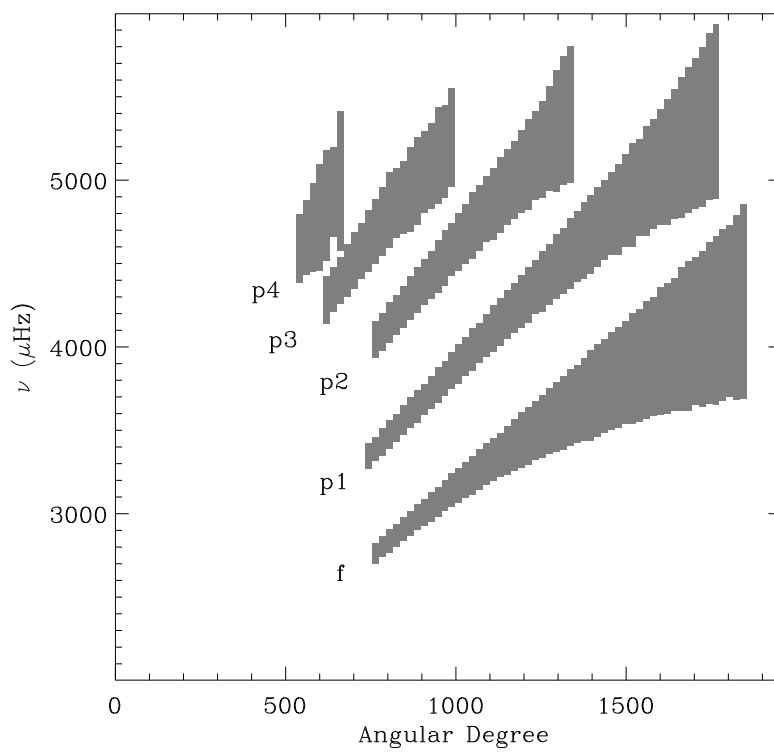


Fig. 1.— Shaded areas of the $\ell - \nu$ plane defining the regions in $\mathbf{k} - \omega$ space where the inversions used MDI Doppler signal.

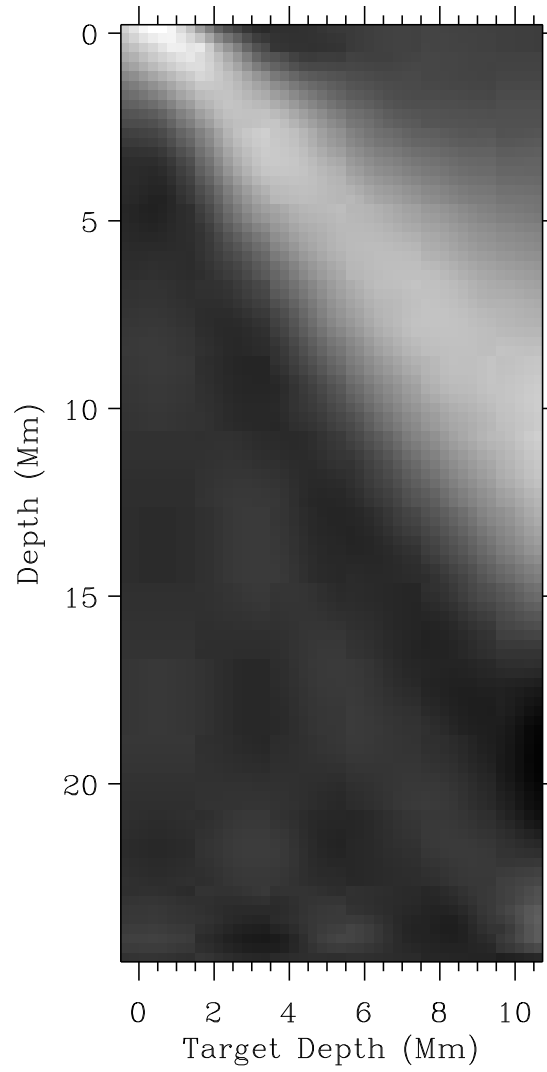


Fig. 2.— Averaging kernel $R(z, z')$, as defined by equation (2), scaled by a linearly increasing function of $|z|$, as a function of depth $|z'|$ for a range of target depths $|z|$. In this example, the wavenumber $q = |\mathbf{q}|$ of the flow corresponds to angular degree approximately 60. The flow is assumed to be steady (i.e., $\sigma = 0$).

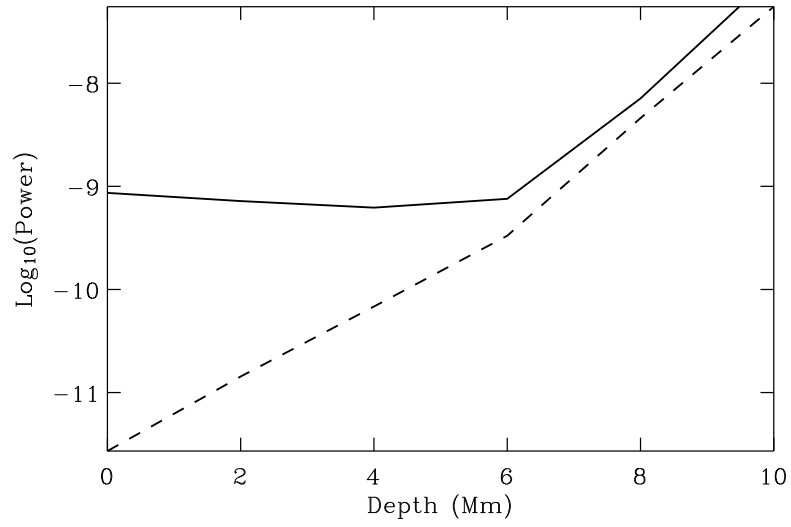


Fig. 3.— Power, in s^{-2} , of the helioseismically-inferred horizontal flow divergence, D , as a function of subphotospheric depth (solid curve). The dashed curve is the expected noise contribution $\mathcal{G}(z)$, defined by equation (5), to the inferred power.

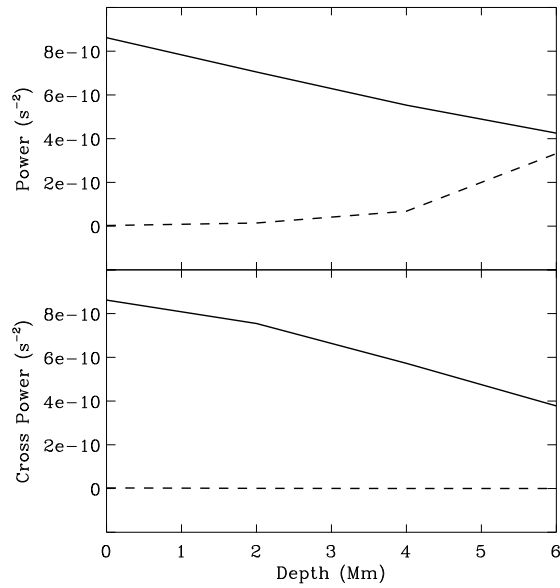


Fig. 4.— Top panel, solid curve: depth dependence of the estimated power in the horizontal flow divergence, after correction for noise. The dashed curve is the noise correction $\mathcal{G}(z)$, replotted from Figure 3. The solid curve in the bottom panel is the estimated cross power (covariance) of the photospheric horizontal flow divergence and the horizontal divergence at depth, as a function of depth. The dashed curve in the bottom panel is the theoretical noise contribution to the cross power, computed similarly to $\mathcal{G}(z)$.

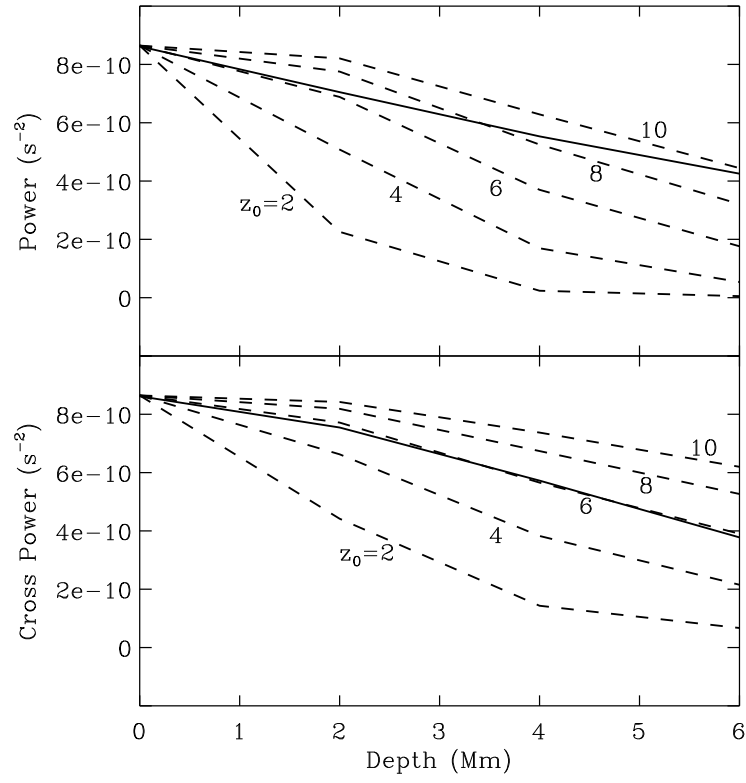


Fig. 5.— Similar to Figure 4, except that the dashed curves are the expected cross power for hypothetical flows of different Gaussian depth, z_0 , as described in the text.